10890 *Biochemistry* **2010,** *49,* 10890–10901
DOI: 10.1021/bi100822q

BIOCHEMISTRY
including biophysical chemistry & molecular biology
Article

Allosteric Regulation of Glycogen Synthase Kinase 3β: A Theoretical Study[†]

Idit Buch,[‡] Dan Fishelovitch,[‡] Nir London,[§] Barak Raveh,[§,∥] Haim J. Wolfson,[∥] and Ruth Nussinov*[,‡,⊥]

[‡]*Department of Human Molecular Genetics and Biochemistry, Sackler Institute of Molecular Medicine, Sackler Faculty of Medicine, Tel Aviv University, Tel Aviv 69978, Israel,* [§]*Department of Microbiology and Molecular Genetics, Institute for Medical Research IMRIC, Faculty of Medicine, Hadassah Medical School, The Hebrew University, POB 12272, Jerusalem 91120, Israel,* [∥]*School of Computer Science, Raymond and Beverly Sackler Faculty of Exact Sciences, Tel Aviv University, Tel Aviv 69978, Israel, and* [⊥]*SAIC-Frederick, Inc., Center for Cancer Research Nanobiology Program, NCI—Frederick, Frederick, Maryland 21702, United States*

Received May 23, 2010; Revised Manuscript Received November 10, 2010

ABSTRACT: Glycogen synthase kinase 3β (GSK-3β) is a serine−threonine kinase belonging to the CMGC family that plays a key role in many biological processes, such as glucose metabolism, cell cycle regulation, and proliferation. Like most protein kinases, GSK-3β is regulated via multiple pathways and sites. We performed all-atom molecular dynamics simulations on the unphosphorylated and phosphorylated unbound GSK-3β and the phosphorylated GSK-3β bound to a peptide substrate, its product, and a derived inhibitor. We found that GSK-3β autophosphorylation at residue Tyr^{216} results in widening of the catalytic groove, thereby facilitating substrate access. In addition, we studied the interactions of the phosphorylated GSK-3β with a substrate and peptide inhibitor located at the active site and observed higher affinity of the inhibitor to the kinase. Furthermore, we detected a potential remote binding site which was previously identified in other kinases. In agreement with experiments we observed that binding of specific peptides at this remote site leads to stabilization of the activation loop located in the active site. We speculate that this stabilization could enhance the catalytic activity of the kinase. We point to this remote site as being structurally conserved and suggest that the allosteric phenomenon observed here may occur in the protein kinase superfamily.

Glycogen synthase kinase 3 (GSK-3)[1] is a ubiquitous serine/threonine kinase that is involved in many biological pathways including glucose metabolism, cell apoptosis, neurological disorders, and heat shock response regulation (*1*, *2*). In contrast to most protein kinases, GSK-3 becomes fully activated upon cellular rest and inhibited at cellular arousal. The kinase is inhibited by external phosphorylation of Ser^{21} in the α isoform and of Ser^{9} in β. Several protein kinases are responsible for this phosphorylation, among them PKA, PKB, and PKC (*3*, *4*). Intriguingly, GSK-3 phosphorylates itself at Tyr^{216}, a residue located at the catalytic site (*5*). This autophosphorylation event causes activation rather than inhibition. Since GSK-3 has multifaceted roles in many signaling pathways, an elevation or relegation of its normal activity level is associated with several diseases, including type II diabetes and neurodegenerative disorders. This makes GSK-3 an important drug target. The majority of the reported GSK-3 inhibitors are ATP analogues or other small drug-like molecules, most of them nonselective (*6*−*12*). Competitive peptide inhibitors selectively target a specific signaling pathway of GSK-3 (*13*). The design of novel potent selective inhibitors depends on detailed structural knowledge and a mechanistic understanding of the substrate−kinase interactions at the substrate binding site (denoted SBS) of the kinase (*14*).

GSK-3 recognizes its substrates by the sequence recognition motif SXXXS(p) (where X stands for any residue and S(p) is a phosphoserine), and it phosphorylates the first serine in this sequence, using an ATP molecule which resides at the catalytic site. The heat shock factor-1 (HSF-1) is a substrate of GSK-3. It is a sequence-specific transcription factor that regulates mammalian heat shock genes at the transcriptional level. Its transcriptional regulatory domain contains the proline-rich sequence KEEPPSPPQSP located at 298−308. Its activity is repressed by the primary phosphorylation of Ser^{307}, carried out by mitogen-activated protein kinase (MAPK). The product, KEEPPSPPQS-(p)P, is next phosphorylated at Ser^{303} by GSK-3 (*15*, *16*), which appears to finalize the inhibition cascade.

Derived from the presumed docking site of the phosphorylated HSF-1 regulatory domain, the substrate-competitive peptide inhibitor L803 was designed with the mutations Glu3Ala and Ser6Ala (*17*). *In vivo* assays demonstrated its antidepressant-like activity (*18*) as well as improvement in glucose homeostasis in ob/ob mice (*19*). The inhibitor, KEAPPAPPQS(p)P, is assumed to interact noncovalently with the key interacting residues of GSK-3β at the SBS by occupying the catalytic groove and preventing the docking of the substrate. Specifically, the negatively charged phosphoserine, Ser10p, interacts electrostatically with positively charged residues Arg^{96}, Arg^{180}, and Lys^{205} (*20*−*22*). Additional information on other key interactions between the inhibitor and GSK-3β is needed to fully understand the mechanism of GSK-3β inhibition as to date there is no

[†]This project has been funded in whole or in part with Federal funds from the National Cancer Institute, National Institutes of Health, under contract number HHSN261200800001E. This research was supported (in part) by the Intramural Research Program of the NIH, National Cancer Institute, Center for Cancer Research.

*Corresponding author. Phone: 301-846-5579. Fax: 301-846-5598. E-mail: ruthnu@helix.nih.gov.

[1]Abbreviations: ABS, allosteric binding site; CDK2, cyclin-dependent kinase 2; GSK-3β, glycogen synthase kinase 3β; HSF-1, heat shock factor-1; MD, molecular dynamics; PKA, cAMP-dependent protein kinase; RMSD, root-mean-square deviations; RMSF, root mean-square fluctuations; SBS, substrate binding site.

 Published on Web 11/24/2010

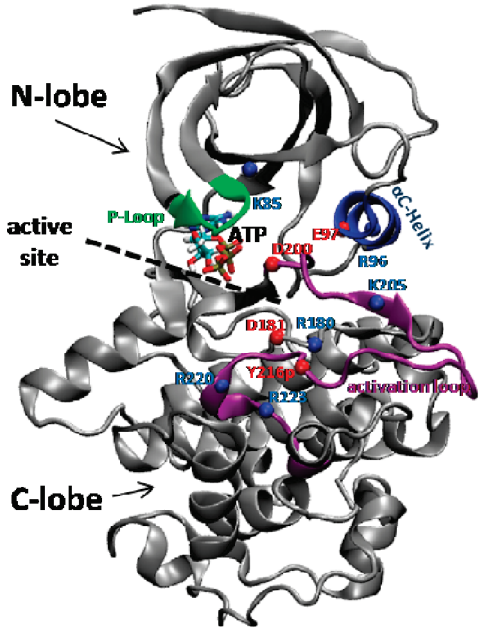

FIGURE 1: The structure of unbound GSK-3β·ATP in ribbon display. The small N-lobe (35−138) and large C-lobe (139−386) are marked. The three regions important for the catalytic activity are highlighted in different colors: the P-loop (64−69) in green, the activation loop (200−226) in purple, and the αC-helix (96−104) in blue. The ATP appears in CPK colors inside its cavity, governed by the P-loop gatekeeper. The residues that govern the activation of GSK-3β appear in beads. These are Arg^{96}, Arg^{180}, and Lys^{205} which comprise the basic binding groove, Asp^{200} and Asp^{181} from the highly conserved motifs DFG (200−202) and HRD (179−181) at the catalytic site, and Glu^{97}, Lys^{85}, and phosphotyrosine Tyr^{216}(p) that are responsible for rendering the enzyme active.

high-resolution structure of GSK-3β bound to one of its protein substrates or protein inhibitors. Figure 1 presents the structure of GSK-3β, highlighting the active site and important regions which govern substrate and inhibitor binding. These include two short motifs inside the catalytic site of the enzyme which are conserved among all species and kinases: HRD (179−181) and DFG (200−202). Both motifs are known to play a crucial role in the catalytic activity of all kinases (*23*).

An open question related to GSK-3β function is how the phosphorylated Tyr^{216} renders the enzyme active. The autophosphorylation event at residue Tyr^{216} causes the kinase to become active, but there is no atomic level description of this activation. This mystery is compounded by the negligible structural difference between the crystal structures of the unphosphorylated (Tyr^{216}) and autophosphorylated (Tyr^{216}(p)) enzyme (*20*, *24*).

To date, several theoretical methodologies were developed to complement experimental observations, to characterize the key interactions of kinases with their substrates and inhibitors, and to predict novel drug candidates. These include feature selection and linear/nonlinear regression (*25*), SAR and QSAR studies (*9*, *12*, *26*), bioinformatics methods (*21*, *27*), pharmacophore characterization (*28*, *29*), and molecular dynamics (MD) simulations (*30*−*32*).

In this study we use MD simulations to elucidate the interactions of GSK-3β with its substrates and inhibitors. By structural and atomistic comparison of the simulated unbound structures of the dephosphorylated (denoted GSK-3β·ATP) and the phosphorylated (denoted GSK-3β(p)·ATP) complexes, we show that the autophosphorylation event at Tyr^{216} is likely to render the kinase active by controlling accessibility. We further perform MD simulations of GSK-3β(p)·ATP bound to the HSF-1 regulatory domain, and to its analogous inhibitor L803, and identify the key residues at the SBS involved in the ligand−enzyme interactions. Finally, we locate a putative allosteric binding site (denoted ABS) at the N-terminal small lobe that is homologous to other kinases and characterize its key interacting residues with the substrate, the inhibitor, and the phosphorylated substrate. We show that substrate and especially phosphorylated substrate binding at the ABS induce distal conformational changes at the catalytic site, toward an activated state of GSK-3β(p). Our findings of substrate allosteric regulation are supported by several experimental studies of other serine−threonine kinases; one of them, CDK2(*33*), is also a member of the CMGC kinase family.

Since protein kinases are key enzymes during the entire cell cycle, their activity is highly regulated. Kinases are turned on or off by phosphorylation (sometimes by the kinase itself), by binding an activator protein, an inhibitor protein, or small molecules. Most kinase activities are regulated via the activation loop located at the active site. To date, only few studies point to remote regulation sites. As a consequence, allosteric regulation mechanisms in kinases are less understood. A hint for allosteric regulation in GSK-3β comes from the finding that the mutation Leu128Ala at the N-lobe, in the PIF-pocket, abolished the phosphorylation of axin that binds at a distal site in the C-lobe (*24*), without affecting the phosphorylation of phosphate-primed substrates (*34*). Here, we aim to gain better insight into allosteric regulation in GSK-3β and how it is linked to the kinase activity. We believe that enhanced mechanistic understanding of the allosteric regulation of GSK-3β will aid rational drug design for this important enzyme.

METHODS

The system setup procedure included modeling of GSK-3β, and of the substrate and peptide inhibitor L803 (*18*, *19*) in the enzyme active site and in the allosteric binding site. These were followed by simulations of the unbound systems (20 ns), and ligand-bound kinase (40 ns). Each bound complex was simulated twice using different starting velocities. All modeling and simulations used the CHARMM27 force field (*35*). Figure 2 summarizes the modeling and simulation flow.

Modeling GSK-3β. The structure of GSK-3β has been solved in complex with different ligands, often surrounding an ATP analogue. Since the Cα RMSD difference between these crystal structures is negligible except for the P-loop (residues 64−69), we utilized several of these structures for modeling. The structure of the unphosphorylated *inactive unbound* enzyme with ATP (apo GSK-3β·ATP) was derived from PDB code 1PYX (*6*), and the existing ATP analogue, ANP, was replaced by ATP using CHARMM (*36*). To model the phosphorylated *active unbound* enzyme with ATP (apo GSK-3β(p)·ATP) (*37*, *38*), the phosphate ion coordinates of Tyr^{216} were taken from the *bound* structure (PDB code 1O9U) (*24*) and added to our unphosphorylated enzyme model. Hydrogens were added using CHARMM (*36*). The model of GSK-3β(p)·ATP was used as a starting point for simulations of the unbound and allosteric bound complexes. The ATP coordinates from the most prevalent conformation of the unbound system were used as a starting point for all bound simulations.

Modeling the Substrate and Inhibitor at the SBS. To date, no crystal structure has been solved for neither the substrate (regulatory domain of HSF-1) nor the inhibitor L803.

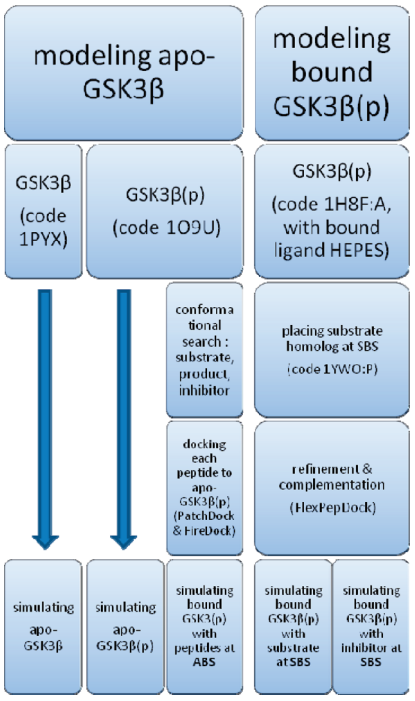

FIGURE 2: Modeling and simulation flow. GSK-3β(p) denotes the phosphorylated kinase at Tyr^{216}. Several X-ray structures are used to model GSK-3β depending on whether it is phosphorylated at Tyr^{216}, and whether it is bound. These structures together with the conformational search, docking procedures, and MD simulation protocol are detailed in the Methods section.

We hypothesized that they bind to the SBS. Modeling these into the active site involved two steps: (1) creation of an N′-truncated, nonphosphorylated substrate based on a template from a solved structure of a similar peptide and (2) docking of this peptide into the binding site using FlexPepDock (*39*), including the addition of the N′ residues and the C′ phosphate ion.

(*1*) *Modeling of an Initial Peptide Conformation in the Substrate Binding Groove*. PDB code 1H8F was chosen as an initial starting structure since the small ligand HEPES (4-(2-hydroxyethyl)-1-piperazineethanesulfonic acid), from the crystallization buffer, has a sulfonate ion bound to the Ser^{10}(p) basic binding pocket of Arg^{96}, Arg^{180}, and Lys^{205} with extensive hydrogen bonds. The phosphate ion of Tyr^{216} and the P-loop were modeled as in 1O9U, where the axin peptide is bound at a distal site away from the active site. The structure of the Slp-76 motif (PDB code 1YWO:P) (*40*) with the sequence PPVPPQRP was next used as a template for our substrate KEEPPSPPQS(p)P. The substrate, truncated at the N′ KEE, was modeled using the backbone of the polyproline Slp-76 motif and was placed such that the Cβ−Oγ bond of Ser^{10} overlaps the sulfonate bond of the HEPES molecule of 1H8F. The rest of the peptide was loosely oriented in the binding cavity. Thus, the starting structure contained 1H8F:A and a truncated substrate placed in its approximate orientation.

(*2*) *Refinement and Complementation of the Peptide Conformation in the Binding Groove Using FlexPepDock*. The starting structure with the peptide in the binding groove was optimized using the FlexPepDock program (*39*), in which the backbone and rigid body orientation of the peptide are optimized iteratively, including on-the-fly side-chain optimization of peptide and enzyme. The simulations were performed with known constraints, including the positioning of Ser^{10} Cβ and Oγ in the phosphate binding pocket and a distance of 3 ± 1 Å between Ser^{6} Oγ and the catalytic Asp^{181} Oδ2 (*23*). In a first step, 100 models were created. Almost all 100 generated models converged to within 1−2 Å peptide backbone RMSD of the starting conformation (Supporting Information Figure S1), and the model with the most extensive hydrogen bonds among the top 5 scoring models was selected. The truncated peptide was modeled first without the N′ (KEE) tail based on the peptide backbone structure that we obtained and high-resolution distance constraints with the binding site. On the other hand, we had no structural information on the tail. Following the model selection, the N′ tail (KEE) was added in an extended conformation (φ/ψ of ±135°) and docked with softer constraints to produce 1000 additional structures, from which the top-scoring model was selected. Finally, phosphate was added to the substrate Ser^{10} and enzyme Tyr^{216} (as the enzyme backbone conformation is fixed during the docking simulations, this phosphate is not expected to affect the overall enzyme conformation), and a short minimization was applied. To model the inhibitor, we mutated the (resulting) substrate structure by E3A and S6A.

Modeling the Substrate and Inhibitor at the ABS. The allosteric binding site was detected when trying to dock the inhibitor onto the kinase using a rigid geometric protein−protein docking procedure, without any distance constraints. This procedure was used to assess the docking solution obtained by FlexPepDock (*39*). Surprisingly, previous experimental works on several kinases from other families have discovered this same allosteric binding site (*41*−*43*). We therefore chose to further explore this site of GSK-3β.

(*1*) *Modeling the Conformation of the Peptide Substrate*. We conducted a conformational search on the substrate, p-substrate (product), and inhibitor using the Cerius2 software (http://www.accelrys.com/products/), after modeling by CHARMM (*36*). Since the five prolines that exist in the peptide ligand introduce strong spatial restraints on the conformation of the 11 amino acid long peptide, we settled for 1000 distinct conformations. We obtained three clusters and picked a representative from each.

(*2*) *Global Search of Peptide Binding Pockets on GSK-3*β. We next applied PatchDock (*44*) followed by FireDock (*45*) to dock the inhibitor onto the enzyme. We chose the top three scoring models for MD simulations. The top scoring solution exhibited a complete geometric fitting throughout the 40 ns simulation, with the inhibitor firmly positioned at the binding site. In the other two solutions, the inhibitor binding to the kinase was not stable, and the simulations halted after 3−4 ns. The docking of the substrate and p-substrate onto the ABS was based on the orientation of the inhibitor bound at the ABS.

Simulations and Analysis. All systems were solvated in a box containing 14625 TIP3P water molecules (*46*), with a minimum margin of 9 Å between the box facets and the solute atoms. To simulate physiological conditions that enable kinase activity, Mg^{2+} ions were added at a concentration of 50 mM, near the ATP, and Cl^{-} ions were added to neutralize the systems. The systems were minimized with the steepest-decent algorithm followed by the adopted basis Newton−Raphson (ABNR) method, gradually decreasing the harmonic force restraints to zero. These setup stages were performed by CHARMM (*36*). Following minimization, the systems were gradually heated to 310 K and equilibrated for 50 ps. The unbound and ligand-bound systems were run for 20 and 40 ns, respectively, using an NVT ensemble with periodic boundary conditions and a time step of 1 fs. The SHAKE algorithm was used to restrain all carbon−hydrogen bonds. Long-range electrostatic interactions were computed

using the particle mesh Ewald summation (*47*). The vdW nonbonded cutoff was set to 12 Å with a smoothing cutoff of 10 Å. Snapshots were saved every 5 ps. The MD simulation protocol including heating, equilibration, and production was carried out by NAMD (*48*).

All snapshots of a simulated complex were grouped into five clusters by the K-means algorithm according to the Cα RMSD difference between the "activation loop", the "αC-helix", and the "P-loop". From the most populated cluster with minimal standard deviation, we picked a snapshot which represents the most visited conformation along the simulation. This conformation was further analyzed and presented in this work. All structural alignments of the obtained GSK-3β conformations with other kinases were done using Multiprot (*49*). All images were produced by VMD (*50*).

RESULTS

The Apo GSK-3β. To obtain atomic level insight into GSK-3β activation, we first modeled the inactive GSK-3β·ATP and the active GSK-3β(p)·ATP (see Methods). These unbound structures were simulated for 20 ns. The final structure of the GSK-3β(p)·ATP simulations served as starting points for further ligand-bound simulations. Figure 3 presents both GSK-3β(p)·ATP and GSK-3β·ATP final structures and highlights important functional sites. We observed that the substrate binding site opens for substrate access in the complex GSK-3β(p)·ATP due to the addition of the phosphate group to Tyr^{216} (Figure 3, left panels) and closes in GSK-3β·ATP where Tyr^{216} is not phosphorylated (Figure 3, right panels). This structural change is mainly governed by three surrounding regions: the αC-helix (residues 96−104), the activation loop (residues 200−226), and the P-loop (residues 64−69). These regions control the closing and opening of the substrate binding site in GSK-3β(p)·ATP and GSK-3β·ATP, respectively. In addition, we monitored intramolecular electrostatic interactions at the active site throughout the simulations (summarized in Supporting Information Table S1). A comparison of the intramolecular interactions in both unbound complexes reveals that in GSK-3β·ATP Arg^{220} interacts with ATP γ-phosphate and Asp^{181} from the conserved HRD motif (residues 179−181), and Arg^{96} interacts with Asp^{200} from the conserved DFG motif (residues 200−202), both in the catalytic site, thus closing the active site. However, in GSK-3β(p)·ATP, Arg^{220} and Arg^{223} are neutralized by Tyr^{216}(p), thus broadening the catalytic groove and enabling full substrate access. Structural analyses show that both the kinase and ATP undergo minor global structural changes (Supporting Information Figure S2). The low root-mean-square deviations (RMSD) of the kinase and ATP in both systems suggest that they can serve as a starting point for further MD simulations with bound ligands.

Peptide Binding at the Substrate Binding Site (SBS). We investigated the key interactions between two peptides: the HSF-1 regulatory domain ("the substrate") and the inhibitor L803 at the enzyme's SBS. Both are 11 amino acids long, and their Ser^{10} residue is phosphorylated. We obtained the N′-truncated, unphosphorylated substrate by homology modeling, docked it in the active site, and added the remaining N′ residues and phosphate group *in situ* (see Methods). The inhibitor model was obtained from the substrate by manual coordinate replacement of Glu3Ala and Ser6Ala. The following two systems were constructed and simulated: $substrate_{SBS}$·GSK-3β(p)·ATP and $inhibitor_{SBS}$·GSK-3β(p)·ATP (subscript "SBS" indicates docking at the SBS). $Substrate_{SBS}$ (or $inhibitor_{SBS}$) was docked with the following binding site putative physicochemical constraints (*51*): (a) close proximity of the ligand Ser^{10}(p) to the kinase Arg^{96}, Arg^{180}, and Lys^{205} at the SBS, and (b) close proximity between the $substrate_{SBS}$ Ser^{6} (to be phosphorylated) and the kinase conserved catalytic Asp^{181}. The latter is known to initiate the catalytic process by attacking the substrate Ser^{6}, thereby forming an alcoholate ion that attacks the ATP γ-phosphate group (*23*). Table 1 summarizes the most significant interactions observed in these systems throughout the simulations. Interestingly, in all systems, both $substrate_{SBS}$ and $inhibitor_{SBS}$ maintain electrostatic interactions between Ser^{10}(p) and the positively charged residues Arg^{96}, Arg^{180}, and Lys^{205} (Figure 4a,b). In addition, the hydrogen bonds and hydrophobic interactions of the proline residues at the peptides' C-terminal end hold throughout the simulations. However, while the N-terminal end of the inhibitor remains intact, the N-terminal end of the substrate departs from its initial location. The Cα RMSD of both peptides (Figure 4c) depicts the structural stability of the inhibitor vs the substrate in the active site.

Both $substrate_{SBS}$ and $inhibitor_{SBS}$ bind to common residues at the SBS, with the inhibitor L803 occupying the same binding groove geometrically, sterically blocking access of any potential substrate. Previously, Ilouz and co-workers modeled the substrate pCREB (*21*) and the GSK-3β N-terminal pseudosubstrate (*52*) bound at the SBS. Comparing the peptide−kinase interactions of both studies and the interactions of HSF-1−GSK-3β(p) or L803−GSK-3β(p) reveals that Arg^{96}, Arg^{180}, and Lys^{205} are the only common amino acids of GSK-3β(p) that interact with the peptides at the SBS, forming electrostatic interactions with the substrate/inhibitor primed phosphate group. Gln^{89} and Asn^{95} which interact with pCREB and are believed to play an important role in substrate and pseudosubstrate recognition do not interact with the HSF-1 fragment or L803. These adopt a fibril-like structure as opposed to the bulkiness of pCREB and GSK-3β N-terminal pseudosubstrate. Therefore, both Gln^{89} and Asn^{95} may not affect HSF-1 or L803 recognition directly. On the other hand, we hypothesize that the conserved Phe^{67}, believed to stabilize the native conformation of the kinase catalytic site for ATP binding, may play the same role upon HSF-1 or L803 binding.

Recently, London et al. (*53*) showed that peptide−protein interactions are dominated by a high number of hydrogen bonds, mainly contributed by peptide backbone atoms. Thus, we measured the average number of hydrogen bonds between the peptides and GSK-3β(p) along the simulations (Supporting Information Figure S3). The results of both Cα RMSD and hydrogen bonds indicate a slightly tighter binding of the inhibitor to the kinase. This observation may stem from electrostatic repulsion between the substrate consecutive Glu^{2} and Glu^{3} which may shift its conformation and therefore interfere with the peptide−substrate binding at the active site. The mutation Glu3Ala in the inhibitor eliminates this repulsion. Additionally, we did not simulate the whole HSF-1 protein (since it has no crystal structure) but only its small regulatory domain; the whole substrate structure may have an impact on the interaction with GSK-3β(p). Nevertheless, our observation is supported by experimental results that showed L803 efficacy as a potential drug (*18*).

Ligand Binding at the Allosteric Binding Site (ABS). (1) Interactions at the ABS. In order to examine the existence of potential binding sites other than the SBS, a different docking

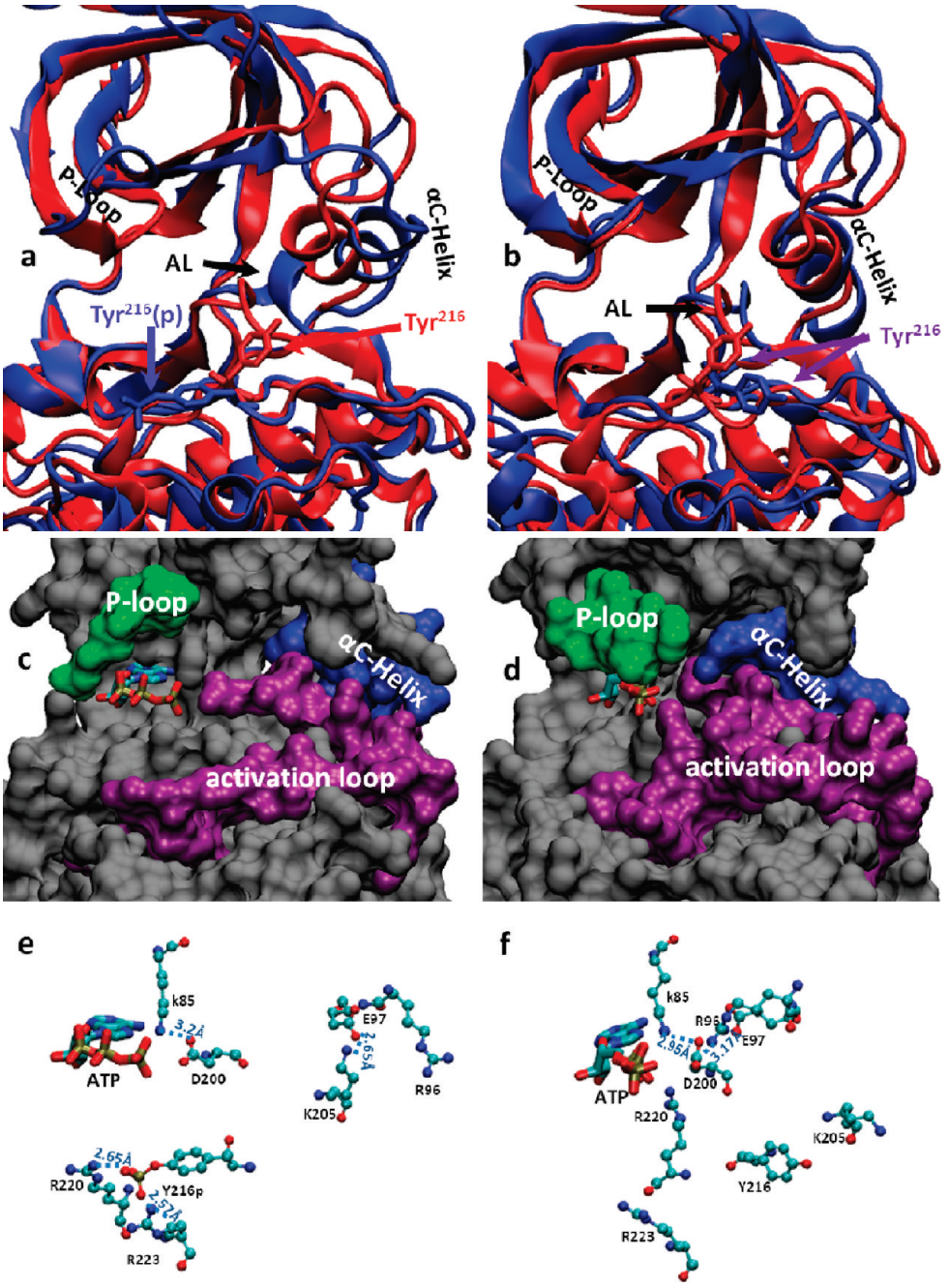

FIGURE 3: The unbound structures of GSK-3β(p)·ATP and GSK-3β·ATP after 20 ns of MD simulations. (a) The final simulation snapshot of GSK-3β(p)·ATP (colored blue) superimposed on the crystal structure of PDB code 1PYX (colored red) from which the simulation originated. (b) The final simulation snapshot of GSK-3β·ATP (colored blue) superimposed on the crystal structure of PDB code 1PYX (colored red) from which the simulation originated. (a) and (b) share the same perspective. The orientation of Tyr^{216} is highlighted. (c) The main structural determinants of the catalytic site of the GSK-3β(p)·ATP system shown in surface representation and colored as follows: the P-loop (residues 64−69) is in green, the activation loop (residues 200−226) is in purple, and the αC-helix (residues 96−104) is in blue. These determinants are in an "open" conformation, creating a wide groove. (d) The main structural determinants of the catalytic site of the GSK-3β·ATP system shown in surface representation and colored as in panel c. The determinants are in a "close" conformation in which the catalytic groove is nearly blocked. (e) Atomic description of the GSK-3β(p)·ATP active site key residues. The phosphotyrosine Tyr^{216}(p) is electrostatically bound to Arg^{220} and Arg^{223}. (f) Atomic description of the GSK-3β·ATP active site key residues. The aromatic ring of Tyr^{216} is headed outside of the cleft, allowing Arg^{220} to interact with the ATP γ-phosphate group and with the highly conserved Asp^{181}.

procedure was applied to GSK-3β(p)·ATP with no constraints (see Methods). The top scoring docking solutions included a new binding site, located at the small lobe, in the vicinity of the activation loop, near the surface of the αC-helix, referred to as "ABS" (see Figure 5). Previous QSAR and modeling studies that examined ATP-noncompetitive inhibitors of GSK-3β based on thiadiazolidinone (TDZD) suggested two putative binding sites: one in the vicinity of the activation loop (similar to our new indicated binding site) and the other in the ATP binding pocket (*9*). Surprisingly, the location of the new binding site was recently identified as a conserved pocket in the protein kinase family (*54*) and was found to be structurally homologous to the PIF pocket of several kinases, where an activator is positioned in the enzyme crystal structures (PDB codes 1FIN, 3HRF, 1OL5, and 1O6L).

Based on our finding of the ABS and given the structural similarities, we simulated three systems: $inhibitor_{ABS}$·GSK-3β(p)·ATP,

Table 1: Interactions at the Substrate Binding Site of Bound GSK-3β

ligand[a]	interactions with GSK-3β(p)
substrate (regulatory domain of HSF-1)	Lys^{1}...Ser^{66} (HB)
	Lys^{1}...Phe^{67} (vdW)
	Glu^{2}...Ser^{66} (HB)
	Glu^{3}...Ser^{66} (HB)
	Ser^{6}...ATP γ-phosphate (HB)
	Gln^{9}...Val^{214},Ile^{217} (vdW)
	Gln^{9}...Arg^{180},Ser^{203} (HB)
	Ser^{10}p...Lys^{94},Arg^{96},Arg^{180},Lys^{205} (Elec)
	Pro^{11}...Lys^{94} (Elec)
inhibitor (L803)	Lys^{1}...Asp^{260} (Elec)
	Glu^{2}...Arg^{220} (Elec)
	Pro^{4}...Arg^{220},Tyr^{221} (HB)
	Pro^{5}...Arg^{220} (vdW)
	Pro^{7}...Ser^{219} (HB)
	Pro^{8}...Ile^{217} (HB)
	Gln^{9}...ATP γ-phosphate (HB)
	Ser^{10}p...Arg^{96},Arg^{180},Lys^{205} (Elec)

[a]The substrate and inhibitor are described in the Methods section.

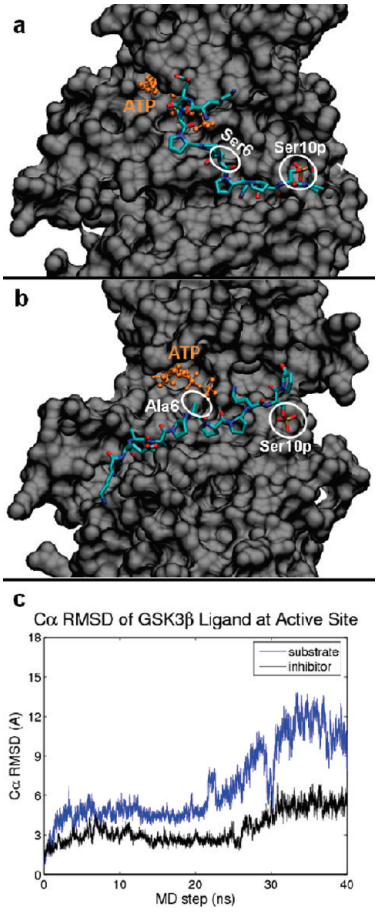

FIGURE 4: Peptide−ligand binding at the substrate binding site (SBS). The snapshots of two ligands bound at the SBS were taken from the most populated cluster of conformations. GSK-3β(p) appears in surface representation, and the ligands appear in sticks. The key interacting residues of the ligands are highlighted. (a) HSF-1 regulatory domain (the substrate) bound at the SBS. The substrate Ser^{6} is the residue due to be phosphorylated by the kinase. (b) The inhibitor L803 bound at the SBS. Alanine replaces Ser^{6} of the substrate. The different surfaces in panels a and b reflect bound and unbound regions. (c) The Cα RMSD of both substrate and inhibitor measured along the 40 ns of simulations.

substrate$_{ABS}$·GSK-3β(p)·ATP, and phosphorylated substrate$_{ABS}$·GSK-3β(p)·ATP (subscript "ABS" denotes docking at the ABS). Figure 5 shows the substrate$_{ABS}$ and phosphorylated substrate$_{ABS}$ bound to GSK-3β(p) (panels a and b of Figure 5, respectively) in the same perspective. Table 2 summarizes the interactions of each of the simulated ligands at the ABS along the simulations. There are two main positively charged sites near or at the surface of αC-helix in GSK-3β(p): Lys^{94} and the adjacent residues Arg^{102} and Lys^{103}. In all ligands Ser^{10}(p) binds to Lys^{103}, or Arg^{102}, or both. The peptide ligands are anchored at Lys^{94} near the surface of the αC-helix by the negatively charged Glu^{2} and Glu^{3}. The presence of another phosphate group on Ser^{6} in a phosphorylated substrate further strengthens the docking of the ligand to the ABS. Based on structural homology of 86% between GSK-3β(p) and CDK2 (both members of the CMGC kinase family), the activator cyclinA binds to CDK2 at approximately the same region as GSK3β(p) binds ligands at the ABS (*33*) (Figure 5c). The figure visualizes the high overlap ratio between the interface of GSK-3β(p)−phosphorylated substrate$_{ABS}$ and CDK2−cyclinA.

Arg^{96}, being an essential residue for phosphate-primed substrates binding at the SBS (*34*), maintains its initial unbound conformation along the simulations of the inhibitor$_{ABS}$ and phosphorylated substrate$_{ABS}$. During the simulation of substrate$_{ABS}$, it reorients toward the bound substrate after 20 ns (Supporting Information Figure S4). As arginine may toggle between a stable and a metastable state during regulation (*55*), the flip may have no effect on subsequent substrate binding at the SBS.

(*2*) *Allosteric Effect of the Peptide Ligands*. To study the cross-talk between the binding of a ligand at the ABS and the active site, we monitored the root-mean-square fluctuations (RMSF) of structural motifs that form the SBS. Figure 6 presents the RMSF of the kinase's main structural determinants in the simulated systems with the unbound system of GSK-3β(p) as a reference. A significant reduction in fluctuations is seen with all tested ligand types at the first nine residues of the activation loop which includes the "magnesium binding loop" (residues 200−205). Ligand binding also affects the αC-helix region where fluctuations of residues 96 and 97 are reduced and stabilized by direct binding of both substrate$_{ABS}$ and p-substrate$_{ABS}$. These results are in accord with Jeffrey et al. (*33*), Yang et al. (*41*), Bayliss et al. (*42*), and Hindie et al. (*43*), who examined the effect of an activator at the PIF binding pocket on the conformation of three regions of the bound kinase: the αC-helix, the G-rich loop, and the activation loop. The authors found that upon binding all three regions are stabilized, adopting an active conformation.

To further understand the differences between the complexes, we analyzed the motion correlation of the kinase Cα atoms along the simulations. Supporting Information Figure S5 displays the cross-correlation maps of the unbound GSK-3β(p) and bound substrate and p-substrate systems. The motion of the N-lobe backbone is autocorrelated over time in all systems, and its cross-correlation increases in the bound systems. This implies that, upon binding, the N-lobe residues move in the same direction to promote catalysis. Interestingly, binding of a ligand at the ABS amplifies the correlation between regions in the enzyme compared to the unbound kinase. The main effect upon substrate and p-substrate binding at the ABS is an amplification of the correlation of motions between the N- and C-lobes. Several regions, such as the catalytic loop (residues 182−187) and the DFG motif (residues 200−202), are correlated with the small lobe as well. However, the hinge between the N- and C-lobes

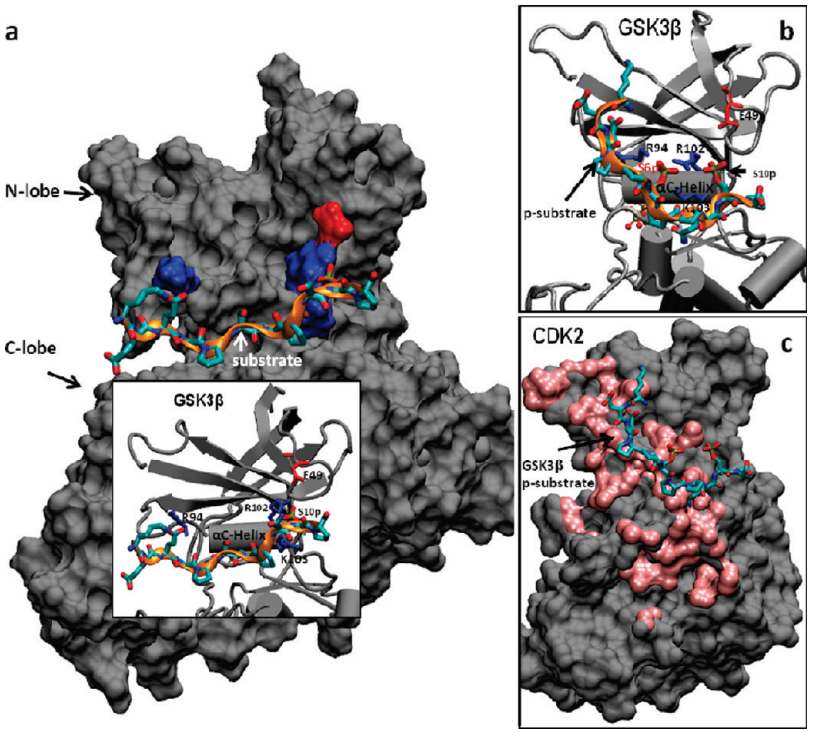

FIGURE 5: Ligand binding at the allosteric binding site (ABS). All complexes were first superimposed, to enable a uniform perspective. (a) GSK-3β(p) in a surface representation, with the substrate (in orange ribbon) bound at the ABS, in the groove between the N-lobe and C-lobe. The positively and negatively charged key interacting residues appear as blue and red spots, respectively. The inset magnifies the interacting residues of the ABS and the substrate and displays the main secondary structures at the N-lobe. The key interacting residues Lys^{94}, Arg^{102}, and Lys^{103} appear from both sides of the αC-helix. (b) Magnification of the interaction between the phosphorylated substrate (the product) and the ABS. The same key interacting residues Lys^{94}, Arg^{102}, and Lys^{103} bind to two negative centers at the p-substrate: S^{6}(p) and S^{10}(p). (c) The phosphorylated substrate (product), as it appears in panel b, being projected on the structural alignment of CDK2 and GSK-3β(p). CDK2 is in surface representation (colored gray), and its residues which are located within 4 Å of the activator protein cyclinA (PDB code 1FIN) are highlighted in pink(*33*). This perspective exhibits the high overlap between the interface product, GSK-3β(p), and the interface cyclinA, CDK2. The structure of GSK-3β(p) is not shown, for clarity.

Table 2: Ligand−GSK-3β Interactions at the Allosteric Binding Site

ligand	key interactions
inhibitor (L803)	Pro^{4}...Arg^{96} (vdW)
	Pro^{5}...Arg^{96} (HB)
	Pro^{7}...Arg^{96},Ile^{100} (vdW)
	Pro^{8}...Phe^{175},Ile^{177} (vdW)
	Gln^{9}...Lys^{103} (HB)
	Ser^{10}p...Lys^{103} (Elec)
	Pro^{11}...Phe^{175},Gln^{365} (vdW)
substrate (regulatory domain of HSF-1)	Glu^{3}...Lys^{94},Arg^{96} (Elec)
	Pro^{4}...Phe^{93},Lys^{205} (vdW)
	Ser^{6}...Arg^{96},Gln^{99}, Gln^{206} (HB)
	Pro^{7}...Gln^{99},Ile^{100} (vdW)
	Pro^{8}...Lys^{103} (HB)
	Ser^{10}p...Arg^{102},Lys^{103} (Elec)
p-substrate (phosphorylated regulatory domain of HSF-1)	Glu^{2}...Ala^{92} (vdW)
	Glu^{3}...Lys^{94} (HB)
	Ser^{6}(p)...Lys^{94},Arg^{102},Lys^{103} (Elec)
	Ser^{6}(p)...Gln^{99} (HB)
	Pro^{7}...Gln^{99},Lys^{103} (HB)
	Gln^{9}...Ile^{177},Phe^{175} (vdW)
	Ser^{10}p...Lys^{102} (Elec)

(residues 134−138), the G-helix (residues 262−273) and the extended loop (residues 285−299), both located at the C-lobe, are anticorrelated with the N-lobe. These correlations are consistent with the catalytic activity of the GSK-3β(p), since the P-loop (residues 64−69), the catalytic loop, and the DFG motif are directly involved in substrate bindings. The cross-correlation map of a substrate bound at the ABS exhibits high similarity to the cross-correlation map published by Cheng et al. (*30*), who analyzed the motions of cAMP-dependent protein kinase (PKA) in complex with a small peptide inhibitor (PDB code 1L3R) (*56*).

(*3*) *Analysis of the Activation Mechanism Induced by Binding at the ABS*. To understand the relation between remote binding at the ABS and catalytic activity, we monitored intramolecular interactions of key functional residues at the active site along the simulations, when the ABS is occupied. Kornev and co-workers (*27*) have discovered an activation mechanism which is conserved in all kinases. According to their findings, the phosphorylation of a residue in the activation loop promotes activation by folding it correctly. Additionally, kinase activation occurs when the αC-helix moves inward toward the catalytic site, such that a tight connection is formed between the two lobes through alignment and stacking of the "hydrophobic spine" (residues Leu^{95}, Leu^{106}, Tyr^{164}, and Phe^{185}), formation of a hydrogen bond in the DFG motif between Asp^{184} and Gly^{186}, and of a salt bridge between Lys^{72} and Glu^{91} (PKA numbering is used). We analyzed the orientation of the corresponding amino acids in GSK-3β(p) in the bound and unbound systems. We aligned the structure of the bound PKA (PDB code 2CPK) (*57*), which is in an active conformation, with bound GSK-3β (PDB code 1H8F) (*20*), focusing on the hydrophobic spine residues (see Figure 7a), the salt bridge, and the hydrogen bond (Figure 7b) within the active site. The RMSD of the corresponding spinal

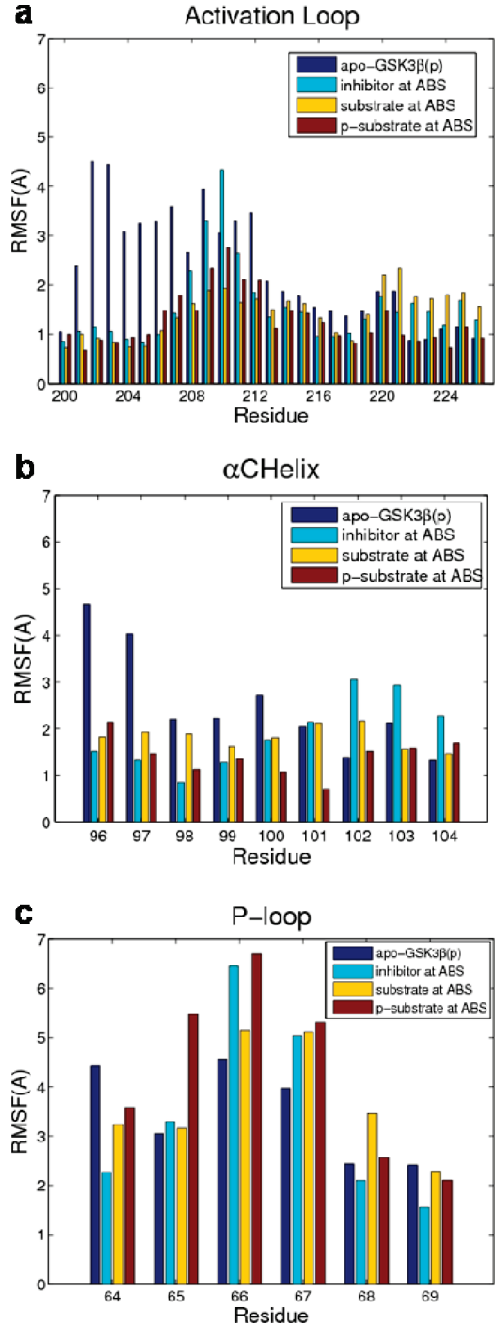

FIGURE 6: The Cα root-mean-square fluctuations (RMSF) of three catalytically important regions measured in all bound complexes at the allosteric binding site. The results were compared to the fluctuations at apo GSK-3β(p). (a) The activation loop. (b) The αC-helix. (c) The P-loop.

residues in GSK-3β (Met^{101}, Leu^{112}, His^{179}, and Phe^{201}) with regard to the bound PKA was very low (0.96 Å). In addition, a hydrogen bond in the DFG motif was found between Asp^{200} and Gly^{202} and a salt bridge between Lys^{85} and Glu^{97}. The congruence of both of these structures combined with the analysis of Kornev et al. (*27*) points to the structure of GSK-3β (PDB code 1H8F) being in an active conformation as well. Thus, a given kinase could be considered as having an active conformation if these properties hold. Figure 8 depicts the spinal RMSD and distance analyses of our systems along the simulations. The spinal residues in apo GSK-3β(p) are completely misaligned, compared to all our bound systems (Figure 8a). As anticipated, both distances Lys^{85}−Glu^{97} (Figure 8b) and Asp^{200}−Gly^{202} (Figure 8c)

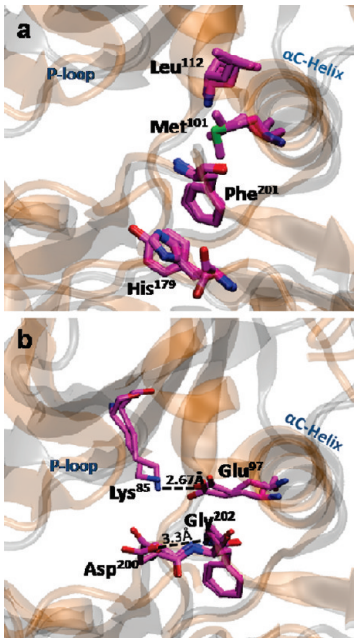

FIGURE 7: Structural alignment between bound PKA (in orange) and GSK-3β(p) (in silver) with highlighted residues of GSK-3β(p) that contribute to the kinase activation state (*27*). (a) The spine residues His^{179}, Phe^{201}, Met^{101}, and Leu^{112}. (b) The salt bridge between Lys^{85} and Glu^{97} (on top), marked in black, and the hydrogen bond between Asp^{200} and the backbone nitrogen of Gly^{202}, marked in green. For clarity, both structures are displayed without hydrogens.

favor a salt bridge and hydrogen bond, respectively, when the substrate was bound at the SBS. The results in systems where the peptide is bound at the ABS are less clear particularly for the inhibitor$_{ABS}$. We further analyzed common representatives from our simulated systems (see Methods) and crystal structures of other kinases with ligand bound at the same allosteric binding site and another allosteric binding site. Table 3 summarizes these results. The crystal structures of PKB and GSK-3β with a bound ligand at their SBS exhibit the lowest spine RMSD (< 1.0 Å). However, the crystal structures of aurora-A, PDK1, and CDK2 with a ligand bound at their ABS have a higher spine RMSD (1.0−1.5 Å). All analyzed crystal structures exhibit a salt bridge in the active site and, except for PDK1, a hydrogen bond within the DFG motif. Noteworthy, the crystal structures of GSK-3β(p) with a bound peptide at another ABS, in the C-lobe, also exhibit low values of spine RMSD and the existence of a salt bridge and a hydrogen bond. Therefore, the crystal structures with a ligand bound at their SBS are considered as active, whereas those with a ligand bound at their ABS are considered "partially" active. The analysis of the simulated bound structures of GSK-3β(p) in this spirit suggests that the *phosphorylated* substrate bound at the ABS could induce partial activation, similar to bound CDK2, whereas a substrate bound at the ABS could render the kinase less active. The inhibitor L803 bound at the ABS could lead to an even lower activity, and the unbound GSK-3β(p) is believed to be practically inactive.

DISCUSSION

Here we conducted MD simulations on unbound and peptide ligand-bound GSK-3β, to investigate substrate and inhibitor binding. We observe that the autophosphorylation of Tyr^{216} renders the kinase active by allowing full substrate accessibility to its active site. The interactions of Tyr^{216}(p) observed here fully

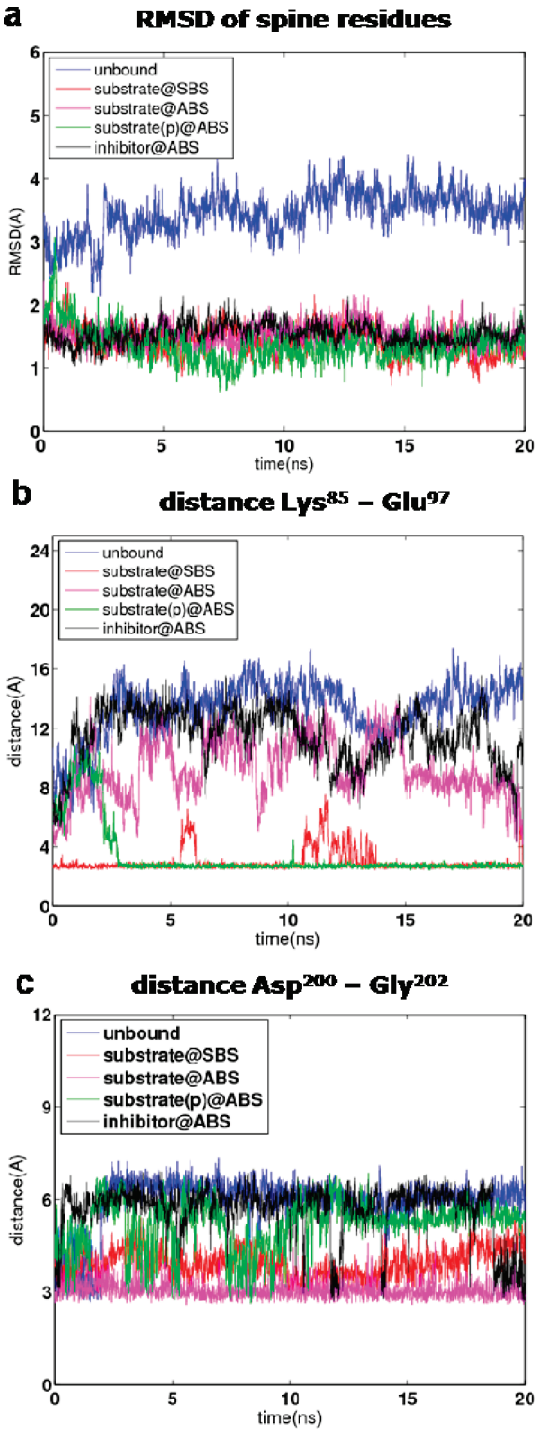

FIGURE 8: Structural analyses of functional residues in the active site along 20 ns of simulations. The trajectories of apo GSK-3β(p) and the bound complexes were compared to the bound GSK-3β(p) crystal structure (PDB code 1H8F). In this bound structure, the spine hydrophobic residues are aligned; there is a salt bridge between Lys^{85} and Glu^{97} and a hydrogen bond between Asp^{200} and Gly^{202}. These indicate an active kinase conformation. (a) All-atom RMSD of the four hydrophobic spine residues Met^{101}, Leu^{112}, His^{179}, and Phe^{201}. A high RMSD indicates an inactive kinase conformation. (b) The distance Lys^{85}–Glu^{97}. A salt bridge is formed at a distance in range (4 Å, 5 Å). Both substrate bound at the SBS and phosphorylated substrate bound at the ABS exhibit a salt bridge throughout the simulation. (c) The distance Asp^{200}–Gly^{202}. A hydrogen bond cutoff is typically less than 3.2 Å. This distance is seen when the substrate was bound at the SBS and at the ABS.

coincide with both experiments of Dajani et al. (*20*) and ter Haar et al. (*22*), who hypothesized that the possible interactions between Tyr^{216}(p) with Arg^{220} and Arg^{223} may stabilize the activation loop and facilitate substrate accessibility.

In general, explicit solvent model MD simulation is a method often used to assess the docking solutions of a ligand and a receptor. A wrong solution often results in the detachment of the ligand from the putative binding site and random movements on the surface of the receptor. The smaller the ligand the higher its flexibility and, therefore, the sooner the detachment occurs, here often within 4 ns. On the other hand, a stable association does not prove the validity of the modeling; it only suggests candidates for experiment to check.

Generally, peptide inhibitors are more selective than small molecule drugs. Previous works have created a template for the design of new substrate-competitive inhibitors for GSK-3β based on the kinase-specific recognition motif SXXXS(p) and on the chemical nature of the regulatory domain of the substrate HSF-1. Based on this template, several potential inhibitors were tested *in vitro* and *in vivo*, and L803 exhibited the highest efficacy (*13*). In this work we first analyzed the key interacting residues at the substrate binding site (SBS) with this regulatory domain (the substrate) and with its derived inhibitor L803. Our results indicated that substrate binding was more flexible along the simulation than the inhibitor binding. Additionally, our structural analysis validates the high affinity of the inhibitor to the kinase. Furthermore, although the L803 is an FDA approved drug for a few years, our work provides atomistic details of its interactions with GSK-3β for the first time.

To date, two binding sites in GSK-3β were revealed experimentally: the substrate binding site and a binding site at the C-lobe where the protein axin binds (*24*). Here we revealed another binding site (the ABS) at the N-lobe, near the surface of the αC-helix. Previously, the mutation Leu128Ala in the ABS was observed to impair the phosphorylation of axin (*34*). Interestingly, similar observations of a remote allosteric binding site in other serine−threonine kinases which belong to different kinase families were reported: (a) in Akt/PKB kinase from the AGC family (28% sequence identity and 70% structural homology) where the phosphorylated hydrophobic motif (HM) at the N-lobe promotes a disorder-to-order transition of the αC-helix leading to an active kinase conformation (*41*); (b) in aurora-A kinase (30% sequence identity and 78% structural homology) belonging to the aurora family, where binding of microtubule-associated protein TPX2 at the same allosteric region causes locking of the active conformation of the kinase (*42*); and (c) in cyclin-dependent kinase CDK2 (34% sequence identity and 86% structural homology) from the CMGC family, as GSK-3β, that becomes partially active after binding of cyclinA at its αC-helix surface (*33*).

On the basis of these observations, we examine the possible effects of a bound ligand at the ABS on the catalytic site and kinase activity. Our findings indicate that peptide binding at the ABS allosterically affects the catalytic site, such that the kinase shifts from its inactive toward its active conformation. These indications are supported by the observations of kinase activity reported by Kornev et al. (*27*), which include the alignment of the spinal residues, a salt bridge, and a hydrogen bond, all in the catalytic site, and a correlated motion of the N-lobe and C-lobe, as previously observed in bound PKA by MD simulation (*30*). The induced formation of the salt bridge within the active site could be the most prominent sign for activation since it brings the αC-helix closer to both the P-loop and activation loop, ready to accept an incoming substrate, thereby increasing the correlation

Table 3: Measures of Activity Level in Kinases

kinase	other components[f]	PDB code (ref)	spine RMSD (Å)[c]	salt bridge (Å)[d]	hydrogen bond (Å)[e]
GSK-3β(p)[a]			2.37	15.44	6.43
GSK-3β(p)[a]	substrate at ABS		1.06	11.59	3.11
GSK-3β(p)[a]	substrate(p) at ABS		1.44	3.37	5.68
GSK-3β(p)[a]	peptide inhibitor at ABS		1.34	13.22	6.56
GSK-3β(p)	peptide activator AXIN at an ABS in the C-lobe	1O9U (*24*)	0.91	3.89	3.41
GSK-3β(p)	peptide inhibitor FRATtide at an ABS in the C-lobe	1GNG (*51*)	1.18	3.60	3.14
CDK2	cyclinA at ABS	1FIN (*33*)	1.30	3.71	3.24
PDK1	small activator at ABS	3HRF (*43*)	1.21	3.46	4.56
aurora-A	peptide at ABS	1OL5 (*42*)	1.26	3.64	3.28
PKB[b]	peptide at SBS	1O6L (*41*)	0.66	3.71	3.22
GSK-3β(p)	small drug at SBS	1H8F (*20*)	0.96	3.55	3.30

[a]Outcome of MD simulation. A representative snapshot was chosen from the most populated conformation. [b]The C-terminal motif of PKB is docked as a pseudoligand at its ABS. [c]RMSD was calculated relative to the spine residues of the active conformation of PKA (PDB code 2CPK). In each residue we considered the backbone atoms as well as Cα, Cβ, and Cδ. [d]The distance was measured between the conserved Lys and Glu in the active site (K85 and E97 in GSK-3β). [e]The distance was measured between Asp and Gly within the conserved DFG motif. [f]ABS, allosteric binding site; SBS, substrate binding site.

of motion between the N-lobe and C-lobe. Our theoretical findings presented in Table 3 support the existence of the ABS as an allosteric regulation site. Together with our analyses of the axin allosteric binding site (*24*, *51*), we hypothesize that GSK-3β, as most (if not all) dynamic proteins (*58*), has few allosteric binding sites, where weak transient bindings can promote activity. Furthermore, since the unbound GSK-3β is inactive, we speculate that binding of an effector at such an allosteric binding site is an essential step for the kinase to become fully active. If the effector is indeed a substrate, the kinase may be subjected to feedback regulation. Nonetheless, while the simulations suggest that our investigated peptides bind at the ABS and induce conformational changes related to partial activation, we cannot overlook the possibility that other (peptide) ligands exhibit this behavior. The characteristics of effective ligands bound at this site are yet to be determined.

Here we provided key interacting residues at the GSK-3β binding sites. Atomic level details of these binding sites may facilitate future discovery of potential drugs. However, additional work is needed to investigate peptide interactions with kinases to achieve high specificity and affinity. Allosteric binding sites are a theme of growing interest (*58*−*61*), and investigation of homologous binding sites in other kinases may lead to increased repertoire of drug design of both small molecules and peptides.

ACKNOWLEDGMENT

We thank Hagit Eldar-Finkelman and Avital Licht-Murava for suggesting this project. We also thank Ora Schueler-Furman for fruitful discussions and assistance with the peptide modeling. All simulations had been performed using the high-performance computational facilities of the Hotspot cluster at the National Cancer Institute, Frederick, MD.

SUPPORTING INFORMATION AVAILABLE

Additional structural analyses of unbound and bound GSK-3β at both substrate and allosteric binding sites along the simulations. This material is available free of charge via the Internet at http://pubs.acs.org.

REFERENCES

1. Grimes, C. A., and Jope, R. S. (2001) The multifaceted roles of glycogen synthase kinase 3beta in cellular signaling. *Prog. Neurobiol. 65*, 391–426.
2. Doble, B. W., and Woodgett, J. R. (2003) GSK-3: tricks of the trade for a multi-tasking kinase. *J. Cell Sci. 116*, 1175–1186.
3. Fang, X., Yu, S. X., Lu, Y., Bast, R. C., Jr., Woodgett, J. R., and Mills, G. B. (2000) Phosphorylation and inactivation of glycogen synthase kinase 3 by protein kinase A. *Proc. Natl. Acad. Sci. U.S.A. 97*, 11960–11965.
4. Shapira, M., Licht, A., Milman, A., Pick, C. G., Shohami, E., and Eldar-Finkelman, H. (2007) Role of glycogen synthase kinase-3beta in early depressive behavior induced by mild traumatic brain injury. *Mol. Cell. Neurosci. 34*, 571–577.
5. Cole, A., Frame, S., and Cohen, P. (2004) Further evidence that the tyrosine phosphorylation of glycogen synthase kinase-3 (GSK3) in mammalian cells is an autophosphorylation event. *Biochem. J. 377*, 249–255.
6. Bertrand, J. A., Thieffine, S., Vulpetti, A., Cristiani, C., Valsasina, B., Knapp, S., Kalisz, H. M., and Flocco, M. (2003) Structural characterization of the GSK-3beta active site using selective and non-selective ATP-mimetic inhibitors. *J. Mol. Biol. 333*, 393–407.
7. Atilla-Gokcumen, G. E., Pagano, N., Streu, C., Maksimoska, J., Filippakopoulos, P., Knapp, S., and Meggers, E. (2008) Extremely tight binding of a ruthenium complex to glycogen synthase kinase 3. *ChemBioChem 9*, 2933–2936.
8. Conde, S., Perez, D. I., Martinez, A., Perez, C., and Moreno, F. J. (2003) Thienyl and phenyl alpha-halomethyl ketones: new inhibitors of glycogen synthase kinase (GSK-3beta) from a library of compound searching. *J. Med. Chem. 46*, 4631–4633.
9. Martinez, A., Alonso, M., Castro, A., Dorronsoro, I., Gelpi, J. L., Luque, F. J., Perez, C., and Moreno, F. J. (2005) SAR and 3D-QSAR studies on thiadiazolidinone derivatives: exploration of structural requirements for glycogen synthase kinase 3 inhibitors. *J. Med. Chem. 48*, 7103–7112.
10. Mohammad, M. K., Al-Masri, I. M., Taha, M. O., Al-Ghussein, M. A., Alkhatib, H. S., Najjar, S., and Bustanji, Y. (2008) Olanzapine inhibits glycogen synthase kinase-3beta: an investigation by docking simulation and experimental validation. *Eur. J. Pharmacol. 584*, 185–191.
11. Prasanna, S., Daga, P. R., Xie, A., and Doerksen, R. J. (2009) Glycogen synthase kinase-3 inhibition by 3-anilino-4-phenylmaleimides: insights from 3D-QSAR and docking. *J. Comput.-Aided Mol. Des. 23*, 113–127.
12. Saitoh, M., Kunitomo, J., Kimura, E., Hayase, Y., Kobayashi, H., Uchiyama, N., Kawamoto, T., Tanaka, T., Mol, C. D., Dougan, D. R., Textor, G. S., Snell, G. P., and Itoh, F. (2009) Design, synthesis and structure-activity relationships of 1,3,4-oxadiazole derivatives as novel inhibitors of glycogen synthase kinase-3beta. *Bioorg. Med. Chem. 17*, 2017–2029.
13. Plotkin, B., Kaidanovich, O., Talior, I., and Eldar-Finkelman, H. (2003) Insulin mimetic action of synthetic phosphorylated peptide inhibitors of glycogen synthase kinase-3. *J. Pharmacol. Exp. Ther.* 974–980.
14. Patel, D. S., Dessalew, N., Iqbal, P., and Bharatam, P. V. (2007) Structure-based approaches in the design of GSK-3 selective inhibitors. *Curr. Protein Pept. Sci. 8*, 352–364.
15. Chu, B., Soncin, F., Price, B. D., Stevenson, M. A., and Calderwood, S. K. (1996) Sequential phosphorylation by mitogen-activated protein kinase and glycogen synthase kinase 3 represses transcriptional activation by heat shock factor-1. *J. Biol. Chem. 271*, 30847–30857.

16. Chu, B., Zhong, R., Soncin, F., Stevenson, M. A., and Calderwood, S. K. (1998) Transcriptional activity of heat shock factor 1 at 37 degrees C is repressed through phosphorylation on two distinct serine residues by glycogen synthase kinase 3 and protein kinases Calpha and Czeta. *J. Biol. Chem. 273*, 18640–18646.
17. Eldar-Finkelman, H., and Ilouz, R. (2003) Challenges and opportunities with glycogen synthase kinase-3 inhibitors for insulin resistance and type 2 diabetes treatment. *Expert Opin. Investig. Drugs 12*, 1511–1519.
18. Kaidanovich-Beilin, O., Milman, A., Weizman, A., Pick, C. G., and Eldar-Finkelman, H. (2004) Rapid antidepressive-like activity of specific glycogen synthase kinase-3 inhibitor and its effect on beta-catenin in mouse hippocampus. *Biol. Psychiatry 55*, 781–784.
19. Kaidanovich-Beilin, O., and Eldar-Finkelman, H. (2006) Long-term treatment with novel glycogen synthase kinase-3 inhibitor improves glucose homeostasis in ob/ob mice: molecular characterization in liver and muscle. *J. Pharmacol. Exp. Ther. 316*, 17–24.
20. Dajani, R., Fraser, E., Roe, S. M., Young, N., Good, V., Dale, T. C., and Pearl, L. H. (2001) Crystal structure of glycogen synthase kinase 3 beta: structural basis for phosphate-primed substrate specificity and autoinhibition. *Cell 105*, 721–732.
21. Ilouz, R., Kowalsman, N., Eisenstein, M., and Eldar-Finkelman, H. (2006) Identification of novel glycogen synthase kinase-3beta substrate-interacting residues suggests a common mechanism for substrate recognition. *J. Biol. Chem. 281*, 30621–30630.
22. ter Haar, E., Coll, J. T., Austen, D. A., Hsiao, H. M., Swenson, L., and Jain, J. (2001) Structure of GSK3beta reveals a primed phosphorylation mechanism. *Nat. Struct. Biol. 8*, 593–596.
23. Johnson, L. N., Noble, M. E., and Owen, D. J. (1996) Active and inactive protein kinases: structural basis for regulation. *Cell 85*, 149–158.
24. Dajani, R., Fraser, E., Roe, S. M., Yeo, M., Good, V. M., Thompson, V., Dale, T. C., and Pearl, L. H. (2003) Structural basis for recruitment of glycogen synthase kinase 3beta to the axin-APC scaffold complex. *EMBO J. 22*, 494–501.
25. Goodarzi, M., Freitas, M. P., and Jensen, R. (2009) Feature selection and linear/nonlinear regression methods for the accurate prediction of glycogen synthase kinase-3beta inhibitory activities. *J. Chem. Inf. Model. 49*, 824–832.
26. Katritzky, A. R., Pacureanu, L. M., Dobchev, D. A., Fara, D. C., Duchowicz, P. R., and Karelson, M. (2006) QSAR modeling of the inhibition of glycogen synthase kinase-3. *Bioorg. Med. Chem. 14*, 4987–5002.
27. Kornev, A. P., Haste, N. M., Taylor, S. S., and Ten Eyck, L. F. (2006) Surface comparison of active and inactive protein kinases identifies a conserved activation mechanism. *Proc. Natl. Acad. Sci. U.S.A. 103*, 17783–17788.
28. Dessalew, N., and Bharatam, P. V. (2006) Investigation of potential glycogen synthase kinase 3 inhibitors using pharmacophore mapping and virtual screening. *Chem. Biol. Drug Des. 68*, 154–165.
29. Kim, H. J., Choo, H., Cho, Y. S., No, K. T., and Pae, A. N. (2008) Novel GSK-3beta inhibitors from sequential virtual screening. *Bioorg. Med. Chem. 16*, 636–643.
30. Cheng, Y., Zhang, Y., and McCammon, J. A. (2006) How does activation loop phosphorylation modulate catalytic activity in the cAMP-dependent protein kinase: a theoretical study. *Protein Sci. 15*, 672–683.
31. Narayanan, A., and Jacobson, M. P. (2009) Computational studies of protein regulation by post-translational phosphorylation. *Curr. Opin. Struct. Biol. 19*, 156–163.
32. Zhang, N., Jiang, Y., Zou, J., Yu, Q., and Zhao, W. (2009) Structural basis for the complete loss of GSK3beta catalytic activity due to R96 mutation investigated by molecular dynamics study. *Proteins 75*, 671–681.
33. Jeffrey, P. D., Russo, A. A., Polyak, K., Gibbs, E., Hurwitz, J., Massague, J., and Pavletich, N. P. (1995) Mechanism of CDK activation revealed by the structure of a cyclinA-CDK2 complex. *Nature 376*, 313–320.
34. Frame, S., Cohen, P., and Biondi, R. M. (2001) A common phosphate binding site explains the unique substrate specificity of GSK3 and its inactivation by phosphorylation. *Mol. Cell 7*, 1321–1327.
35. Mackerell, A. D., Jr., Feig, M., and Brooks, C. L., III (2004) Extending the treatment of backbone energetics in protein force fields: limitations of gas-phase quantum mechanics in reproducing protein conformational distributions in molecular dynamics simulations. *J. Comput. Chem. 25*, 1400–1415.
36. Brooks, B. R., Brooks, C. L., III, Mackerell, A. D., Jr., Nilsson, L., Petrella, R. J., Roux, B., Won, Y., Archontis, G., Bartels, C., Boresch, S., Caflisch, A., Caves, L., Cui, Q., Dinner, A. R., Feig, M., Fischer, S., Gao, J., Hodoscek, M., Im, W., Kuczera, K., Lazaridis, T., Ma, J., Ovchinnikov, V., Paci, E., Pastor, R. W., Post, C. B., Pu, J. Z., Schaefer, M., Tidor, B., Venable, R. M., Woodcock, H. L., Wu, X., Yang, W., York, D. M., and Karplus, M. (2009) CHARMM: the biomolecular simulation program. *J. Comput. Chem. 30*, 1545–1614.
37. Hughes, K., Nikolakaki, E., Plyte, S. E., Totty, N. F., and Woodgett, J. R. (1993) Modulation of the glycogen synthase kinase-3 family by tyrosine phosphorylation. *EMBO J. 12*, 803–808.
38. Wang, Q. M., Fiol, C. J., DePaoli-Roach, A. A., and Roach, P. J. (1994) Glycogen synthase kinase-3 beta is a dual specificity kinase differentially regulated by tyrosine and serine/threonine phosphorylation. *J. Biol. Chem. 269*, 14566–14574.
39. Raveh, B., London, N., and Schueler-Furman, O. (2010) Sub-angstrom modeling of complexes between flexible peptides and globular proteins, *Proteins* 78, 2029−2040.
40. Deng, L., Velikovsky, C. A., Swaminathan, C. P., Cho, S., and Mariuzza, R. A. (2005) Structural basis for recognition of the T cell adaptor protein SLP-76 by the SH3 domain of phospholipase Cgamma1. *J. Mol. Biol. 352*, 1–10.
41. Yang, J., Cron, P., Good, V. M., Thompson, V., Hemmings, B. A., and Barford, D. (2002) Crystal structure of an activated Akt/protein kinase B ternary complex with GSK3-peptide and AMP-PNP. *Nat. Struct. Biol. 9*, 940–944.
42. Bayliss, R., Sardon, T., Vernos, I., and Conti, E. (2003) Structural basis of Aurora-A activation by TPX2 at the mitotic spindle. *Mol. Cell 12*, 851–862.
43. Hindie, V., Stroba, A., Zhang, H., Lopez-Garcia, L. A., Idrissova, L., Zeuzem, S., Hirschberg, D., Schaeffer, F., Jorgensen, T. J., Engel, M., Alzari, P. M., and Biondi, R. M. (2009) Structure and allosteric effects of low-molecular-weight activators on the protein kinase PDK1. *Nat. Chem. Biol. 5*, 758–764.
44. Schneidman-Duhovny, D., Inbar, Y., Nussinov, R., and Wolfson, H. J. (2005) PatchDock and SymmDock: servers for rigid and symmetric docking. *Nucleic Acids Res. 33*, W363–367.
45. Mashiach, E., Schneidman-Duhovny, D., Andrusier, N., Nussinov, R., and Wolfson, H. J. (2008) FireDock: a web server for fast interaction refinement in molecular docking. *Nucleic Acids Res. 36*, W229–232.
46. Jorgensen, W. L., Chandrasekhar, J., Madura, J. D., Impey, R. W., and Klein, M. L. (1983) Comparison of simple potential functions for simulating liquid water. *J. Chem. Phys.,* 79.
47. York, D. M., Wlodawer, A., Pedersen, L. G., and Darden, T. A. (1994) Atomic-level accuracy in simulations of large protein crystals. *Proc. Natl. Acad. Sci. U.S.A. 91*, 8715–8718.
48. Phillips, J. C., Braun, R., Wang, W., Gumbart, J., Tajkhorshid, E., Villa, E., Chipot, C., Skeel, R. D., Kale, L., and Schulten, K. (2005) Scalable molecular dynamics with NAMD. *J. Comput. Chem. 26*, 1781–1802.
49. Shatsky, M., Nussinov, R., and Wolfson, H. J. (2004) A method for simultaneous alignment of multiple protein structures. *Proteins 56*, 143–156.
50. Humphrey, W., Dalke, A., and Schulten, K. (1996) VMD: visual molecular dynamics. *J. Mol. Graphics 14* (33−38), 27–38.
51. Bax, B., Carter, P. S., Lewis, C., Guy, A. R., Bridges, A., Tanner, R., Pettman, G., Mannix, C., Culbert, A. A., Brown, M. J., Smith, D. G., and Reith, A. D. (2001) The structure of phosphorylated GSK-3beta complexed with a peptide, FRATtide, that inhibits beta-catenin phosphorylation. *Structure 9*, 1143–1152.
52. Ilouz, R., Pietrokovski, S., Eisenstein, M., and Eldar-Finkelman, H. (2008) New insights into the autoinhibition mechanism of glycogen synthase kinase-3beta. *J. Mol. Biol. 383*, 999–1007.
53. London, N., Movshovitz-Attias, D., and Schueler-Furman, O. (2010) The structural basis of peptide-protein binding strategies. *Structure 18*, 188–199.
54. Thompson, E. E., Kornev, A. P., Kannan, N., Kim, C., Ten Eyck, L. F., and Taylor, S. S. (2009) Comparative surface geometry of the protein kinase family. *Protein Sci. 18*, 2016–2026.
55. Oprea, T. I., Hummer, G., and Garcia, A. E. (1997) Identification of a functional water channel in cytochrome P450 enzymes. *Proc. Natl. Acad. Sci. U.S.A. 94*, 2133–2138.
56. Madhusudan, Akamine, P., Xuong, N. H., and Taylor, S. S. (2002) Crystal structure of a transition state mimic of the catalytic subunit of cAMP-dependent protein kinase. *Nat. Struct. Biol. 9*, 273–277.

57. Knighton, D. R., Zheng, J. H., Ten Eyck, L. F., Ashford, V. A., Xuong, N. H., Taylor, S. S., and Sowadski, J. M. (1991) Crystal structure of the catalytic subunit of cyclic adenosine monophosphate-dependent protein kinase. *Science 253*, 407–414.
58. Gunasekaran, K., Ma, B., and Nussinov, R. (2004) Is allostery an intrinsic property of all dynamic proteins? *Proteins 57*, 433–443.
59. del Sol, A., Tsai, C. J., Ma, B., and Nussinov, R. (2009) The origin of allosteric functional modulation: multiple pre-existing pathways. *Structure 17*, 1042–1050.
60. Goodey, N. M., and Benkovic, S. J. (2008) Allosteric regulation and catalysis emerge via a common route. *Nat. Chem. Biol. 4*, 474–482.
61. Cui, Q., and Karplus, M. (2008) Allostery and cooperativity revisited. *Protein Sci. 17*, 1295–1307.